COMMUNICATIONS IN COMPUTATIONAL PHYSICS
Vol. **5**, No. 2-4, pp. 821-835

Commun. Comput. Phys.
February 2009

Application of the Local Discontinuous Galerkin Method for the Allen-Cahn/Cahn-Hilliard System

Yinhua Xia[1], Yan Xu[1] and Chi-Wang Shu[2,*]

[1] *Department of Mathematics, University of Science and Technology of China, Hefei, Anhui 230026, China.*
[2] *Division of Applied Mathematics, Brown University, Providence, RI 02912, USA.*

Received 12 September 2007; Accepted (in revised version) 6 February 2008

Available online 1 August 2008

Abstract. In this paper, we consider the application of the local discontinuous Galerkin method for the Allen-Cahn/Cahn-Hilliard system. The method in this paper extends the local discontinuous Galerkin method in [10] to the more general application system which is coupled with the Allen-Cahn and Cahn-Hilliard equations. Similar energy stability result as that in [10] is presented. Numerical results for the nonlinear problems which include the Allen-Cahn/Cahn-Hilliard system for one-dimensional and two-dimensional cases demonstrate the accuracy and capability of the numerical method.

AMS subject classifications: 65M60, 35K55

Key words: Allen-Cahn/Cahn-Hilliard system, local discontinuous Galerkin method, free energy, stability.

1 Introduction

In this paper, we consider the extension of the local discontinuous Galerkin (LDG) method in [10] for the more general Allen-Cahn/Cahn-Hilliard (AC/CH) system in $\Omega \in \mathbb{R}^d$ ($d \leq 3$)

$$\begin{cases} u_t = \nabla \cdot [b(u,v)\nabla(\Psi_u(u,v) - \gamma \Delta u)], \\ \rho v_t = -b(u,v)[\Psi_v(u,v) - \gamma \Delta v], \end{cases} \tag{1.1}$$

where γ, ρ are given constants. The mobility, $b(u,v)$, is assumed to be nonnegative and to vanish at the "pure phases" (i.e., $u = 0$ or $u = 1$). This assumption, which reflects divergence of the time scale in a minimal entropy completely ordered system, implies

*Corresponding author. *Email addresses:* xiayh@mail.ustc.edu.cn (Y. Xia), yxu@ustc.edu.cn (Y. Xu), shu@dam.brown.edu (C.-W. Shu)

degeneracy of the parabolic system (1.1). The homogeneous free energy, Ψ, will be assumed to contain two terms, one which reflects entropy contribution and another which accounts for the energy of mixing.

In [10], we developed the LDG methods for the Cahn-Hilliard equations which use the discontinuous, piecewise polynomial as the solution and test functions. In this paper, we extend the techniques in [10] to devise an LDG method for the AC/CH system (1.1) and state similar energy stability result as that in [10]. The Cahn-Hilliard equations considered in [10] is a special case of the AC/CH system (1.1) when we set the initial condition with $v=0$. Numerical simulation results demonstrate that the LDG method is a very powerful method for solving this type of fully nonlinear problems.

A systematic derivation of the system (2.1) has been given by Cahn and Novick-Cohen [3], based on energetic exchange probabilities for a Fe-Al binary alloy system on a large but finite BCC lattice. The conserved and non-conserved order parameters u and v may be defined as

$$u(\boldsymbol{n})=\frac{1}{2N}\sum_{\boldsymbol{a}\in\boldsymbol{A}}c(\boldsymbol{n}+\boldsymbol{a})+c(\boldsymbol{n}),\quad v(\boldsymbol{n})=\frac{1}{2N}\sum_{\boldsymbol{a}\in\boldsymbol{A}}c(\boldsymbol{n}+\boldsymbol{a})-c(\boldsymbol{n}),$$

where $c(\boldsymbol{n})$ represents the probability of finding an Fe atom at site $\boldsymbol{n}$ of a given lattice segments and $\boldsymbol{A}$ represents the set of nearest neighbors with $\boldsymbol{N}=|\boldsymbol{A}|$. Thus the u and v of the system (2.1) satisfy the constrains

$$u\in[0,1],\quad v\in[-\frac{1}{2},\frac{1}{2}],\quad (u\pm v)\in[0,1]. \tag{1.2}$$

In [1,2], mixed finite element methods have been developed to approximate the AC/CH system and C^0 basis functions are used.

The discontinuous Galerkin (DG) method we discuss in this paper is a class of finite element methods using completely discontinuous piecewise polynomial space for the numerical solution and the test functions in the spatial variables. DG methods are well suited for parallel computing and *hp*-adaptation, which consists of local mesh refinement and/or the adjustment of the polynomial order in individual elements. More general information about DG methods can be found in [4,6–8].

The main motivation for the algorithm discussed in [10] and generalized in this paper originates from the LDG techniques which have been developed for convection diffusion equations (containing second derivatives) [5] and nonlinear wave equations with high order derivatives (e.g. in [9,11–13]). In these papers, stable LDG methods for quite general nonlinear wave equations including multi-dimensional and system cases have been developed. The proof of the nonlinear L^2 stability of these methods are usually given and successful numerical experiments demonstrate their capability. These results indicate that the LDG method is a good tool for solving nonlinear equations in mathematical physics.

The outline of this paper is as follows. In Section 2, we review the properties of the AC/CH system and important application areas for this system. In Section 3, we present

and analyze the LDG methods for the AC/CH system. Section 4 contains numerical results for the nonlinear problems which include the AC/CH system for one-dimensional and two-dimensional cases. The numerical results demonstrate the accuracy and capability of the LDG methods. Concluding remarks are given in Section 5.

2 The AC/CH system

The Allen-Cahn/Cahn-Hilliard system was developed in [3] to model simultaneous phase separation and ordering in binary alloys. The AC/CH system on a bounded domain $\Omega\in\mathcal{R}^d$ $(d\leq 3)$ is

$$u_t=\nabla\cdot(b(u,v)\nabla\frac{\delta\mathcal{E}}{\delta u}), \tag{2.1a}$$

$$\rho v_t=-b(u,v)\frac{\delta\mathcal{E}}{\delta v}, \tag{2.1b}$$

where the degenerate mobility is

$$b(u,v)=u(1-u)(\frac{1}{4}-v^2), \tag{2.2}$$

and the free energy is given by

$$\mathcal{E}(u,v)=\int_\Omega\Big\{\frac{\gamma}{2}(|\nabla u|^2+|\nabla v|^2)+\Psi(u,v)\Big\}dx. \tag{2.3}$$

The homogeneous free energy $\Psi(u,v)$ is

$$\Psi(u,v)=\theta[\Phi(u+v)+\Phi(u-v)]+\frac{1}{2}\left[\alpha u(1-u)-\beta v^2\right], \tag{2.4}$$

$$\Phi(s)=s\ln s+(1-s)\ln(1-s). \tag{2.5}$$

Here θ represents the temperature, γ is the coefficient of gradient energy and α, β are the coefficients of nearest and next-nearest neighbors pairwise energetic interactions.

In the AC/CH system, u denotes an average concentration and v represents a non-conserved order variable. Neumann boundary conditions are prescribed for u, v and no-flux boundary for the mass flux $J=-b(u,v)\nabla w$, i.e.,

$$\frac{\partial u}{\partial\nu}=\frac{\partial v}{\partial\nu}=b(u,v)\frac{\partial w}{\partial\nu}=0\quad\text{on }\partial\Omega, \tag{2.6}$$

where $w=\delta\mathcal{E}/\delta u$ is the chemical potential and ν is the normal vector to $\partial\Omega$. From this boundary condition, we have

$$\frac{d}{dt}\int_\Omega u d\boldsymbol{x}=0,\quad\frac{d}{dt}\mathcal{E}(u,v)\leq 0. \tag{2.7}$$

When we choose the initial condition $u^0 \equiv \frac{1}{2}$, which yields that $\Psi_u \equiv 0$ and $u \equiv \frac{1}{2}$, the system (2.1) collapses to a logarithmic Allen-Cahn equation. Whereas, when we choose $v^0 \equiv 0$, which yields that $\Psi_v = 0$, the system (2.1) collapses to a logarithmic Cahn-Hilliard equation considered in [10]. Therefore, the system (2.1) can be considered as a system encompassing both the Allen-Cahn and Cahn-Hilliard equations. The AC/CH system is studied to model further aspects of the behavior of alloys and related physical systems, when coupled with equations of fluid flow or heat conduction, etc.

3 The LDG method for the AC/CH system

In this section, we consider the LDG method for the AC/CH system (1.1) in $\Omega \in \mathbb{R}^d$ with $d \leq 3$. Although we do not perform numerical experiments in three dimensions in this paper, the LDG methods and the energy stability results of this paper are valid for all $d \leq 3$.

3.1 Notation

Let $\mathcal{T}_h$ denote a tessellation of Ω with shape-regular elements K. Let Γ denote the union of the boundary faces of elements $K \in \mathcal{T}_h$, i.e., $\Gamma = \cup_{K\in\mathcal{T}_h} \partial K$, and $\Gamma_0 = \Gamma \backslash \partial\Omega$.

In order to describe the flux functions we need to introduce some notations. Let e be a face shared by the "left" and "right" elements K_L and K_R (we refer to [13] and [10] for a proper definition of "left" and "right" in our context). Define the normal vectors ν_L and ν_R on e pointing exterior to K_L and K_R, respectively. If ψ is a function on K_L and K_R, but possibly discontinuous across e, let ψ_L denote $(\psi|_{K_L})|_e$ and ψ_R denote $(\psi|_{K_R})|_e$ the left and right trace, respectively.

Let $\mathcal{P}^p(K)$ be the space of polynomials of degree at most $p \geq 0$ on $K \in \mathcal{T}_h$. The finite element spaces are denoted by

$$V_h = \Big\{ \varphi :\ \varphi|_K \in \mathcal{P}^p(K),\ \ \forall K \in \mathcal{T}_h \Big\},$$
$$\Sigma_h = \Big\{ \boldsymbol{\eta} = (\eta_1, \cdots, \eta_d)^T :\ \eta_l|_K \in \mathcal{P}^p(K),\, l = 1 \cdots d,\ \forall K \in \mathcal{T}_h \Big\}.$$

Note that functions in V_h and Σ_h are allowed to have discontinuities across element interfaces.

3.2 The LDG methods

First, we rewrite (2.1) as a first order system

$$u_t = \nabla \cdot \boldsymbol{s}_1, \quad v_t = -b(u,v)(-q_2 + r_2)/\rho, \quad \boldsymbol{s}_1 = b(u,v)\boldsymbol{p}, \tag{3.1a}$$
$$\boldsymbol{p} = \nabla(-q_1 + r_1), \quad q_1 = \gamma \nabla \cdot \boldsymbol{w}_1, \quad q_2 = \gamma \nabla \cdot \boldsymbol{w}_2, \tag{3.1b}$$
$$\boldsymbol{w}_1 = \nabla u, \quad \boldsymbol{w}_2 = \nabla v, \quad r_1 = \Psi_u, \quad r_2 = \Psi_v, \tag{3.1c}$$

where $\Psi_u=\partial\Psi/\partial u$ and $\Psi_v=\partial\Psi/\partial v$. Applying the LDG method to the system (3.1), we have the scheme: Find u, v, q_1, q_2, r_1, $r_2\in V_h$ and $\boldsymbol{s}_1$, $\boldsymbol{p}$, $\boldsymbol{w}_1$, $w_2\in\Sigma_h$, such that, for all test functions φ_1, φ_2, φ_3, φ_4, φ_5, $\varphi_6\in V_h$ and $\boldsymbol{\eta}_1$, $\boldsymbol{\eta}_2$, $\boldsymbol{\eta}_3$, $\boldsymbol{\eta}_4\in\Sigma_h$, we have

$$\int_K u_t\varphi_1 dK=-\int_K \boldsymbol{s}_1\cdot\nabla\varphi_1 dK+\int_{\partial K}\widehat{\boldsymbol{s}_1\cdot\nu}\varphi_1 ds, \tag{3.2a}$$

$$\int_K v_t\varphi_2 dK=\int_K -b(u,v)(-q_2+r_2)\varphi_2/\rho dK, \tag{3.2b}$$

$$\int_K \boldsymbol{s}_1\cdot\boldsymbol{\eta}_1 dK=\int_K b(u,v)\boldsymbol{p}\cdot\boldsymbol{\eta}_1 dK, \tag{3.2c}$$

$$\int_K \boldsymbol{p}\cdot\boldsymbol{\eta}_2 dK=-\int_K(-q_1+r_1)(\nabla\cdot\boldsymbol{\eta}_2)dK+\int_{\partial K}(-\widehat{q_1}+\widehat{r_1})(\boldsymbol{\eta}_2\cdot\nu)ds, \tag{3.2d}$$

$$\int_K q_1\varphi_3 dK=-\gamma\int_K \boldsymbol{w}_1\cdot\nabla\varphi_3 dK+\int_{\partial K}\gamma\widehat{\boldsymbol{w}_1\cdot\nu}\varphi_3 ds, \tag{3.2e}$$

$$\int_K q_2\varphi_4 dK=-\gamma\int_K \boldsymbol{w}_2\cdot\nabla\varphi_4 dK+\int_{\partial K}\gamma\widehat{\boldsymbol{w}_2\cdot\nu}\varphi_4 ds, \tag{3.2f}$$

$$\int_K \boldsymbol{w}_1\cdot\boldsymbol{\eta}_3 dK=-\int_K u(\nabla\cdot\boldsymbol{\eta}_3)dK+\int_{\partial K}\widehat{u}(\boldsymbol{\eta}_3\cdot\nu)ds, \tag{3.2g}$$

$$\int_K \boldsymbol{w}_2\cdot\boldsymbol{\eta}_4 dK=-\int_K v(\nabla\cdot\boldsymbol{\eta}_4)dK+\int_{\partial K}\widehat{v}(\boldsymbol{\eta}_4\cdot\nu)ds, \tag{3.2h}$$

$$\int_K r_1\varphi_5 dK=\int_K \Psi_u\varphi_5 dK,\quad \int_K r_2\varphi_6 dK=\int_K \Psi_v\varphi_6 dK. \tag{3.2i}$$

The "hat" terms in (3.2) in the cell boundary terms from integration by parts are the so-called "numerical fluxes", which are functions defined on the edges and should be designed based on different guiding principles for different PDEs to ensure stability. Similar to the development in [10], it turns out that we can take the simple choices such that

$$\begin{aligned}&\widehat{\boldsymbol{s}_1}|_e=\boldsymbol{s}_{1L},\quad \widehat{q_1}|_e=q_{1R},\quad \widehat{r_1}|_e=r_{1R},\\&\widehat{\boldsymbol{w}_1}|_e=\boldsymbol{w}_{1L},\quad \widehat{u}|_e=u_R,\quad \widehat{\boldsymbol{w}_2}|_e=\boldsymbol{w}_{2L},\quad \widehat{v}|_e=v_R.\end{aligned} \tag{3.3}$$

By the boundary conditions (2.6), we take

$$\widehat{\boldsymbol{s}}_1=\boldsymbol{0},\quad \widehat{q}_1=q_1^{in},\quad \widehat{r}_1=r_1^{in},\quad \widehat{\boldsymbol{w}}_1=\boldsymbol{0},\quad \widehat{\boldsymbol{w}}_2=\boldsymbol{0},\quad \widehat{u}=u^{in},\quad \widehat{v}=v^{in} \tag{3.4}$$

at the domain boundary, where u^{in} means the value taking from the inside of the boundary element. We remark that the numerical solution of u is conserved under this boundary condition, easily seen by set $\phi_1=1$ in (3.2a). We also remark that the choice for the fluxes (3.3) is not unique. In fact the crucial part is taking $\widehat{\boldsymbol{s}_1}$ and $\widehat{q_1}$,$\widehat{r_1}$ from opposite sides, $\widehat{\boldsymbol{w}_1}$ and $\widehat{u}$ from opposite sides and $\widehat{\boldsymbol{w}_2}$ and $\widehat{v}$ from opposite sides.

3.3 Energy stability

Proposition 3.1. (Energy stability) The solution to the schemes (3.2) and the flux satisfies the energy stability

$$\frac{d}{dt}\int_\Omega \Big\{\frac{\gamma}{2}(\boldsymbol{w}_1\cdot\boldsymbol{w}_1+\boldsymbol{w}_2\cdot\boldsymbol{w}_2)+\Psi(u,v)\Big\}dx\le 0.$$

Proof. Choosing the test function $\varphi_5=-u_t$ and $\varphi_6=-v_t$ in (3.2i), we obtain

$$-\int_K r_1u_t dK=-\int_K \Psi_u u_t dK,\quad -\int_K r_2v_t dK=-\int_K \Psi_v v_t dK. \tag{3.5}$$

After taking the time derivative, we choose the test functions $\boldsymbol{\eta}_3=\boldsymbol{w}_1$, in (3.2g) and $\boldsymbol{\eta}_4=\boldsymbol{w}_2$ in (3.2h). Then we get

$$\gamma\int_K \boldsymbol{w}_{1t}\cdot\boldsymbol{w}_1 dK=-\gamma\int_K u_t(\nabla\cdot\boldsymbol{w}_1)dK+\gamma\int_{\partial K}\widehat{u_t}(\boldsymbol{w}_1\cdot\nu)ds, \tag{3.6}$$

$$\gamma\int_K \boldsymbol{w}_{2t}\cdot\boldsymbol{w}_2 dK=-\gamma\int_K v_t(\nabla\cdot\boldsymbol{w}_2)dK+\gamma\int_{\partial K}\widehat{v_t}(\boldsymbol{w}_2\cdot\nu)ds. \tag{3.7}$$

For (3.2a)-(3.2f), we take the test functions

$$\varphi_1=-q_1+r_1,\quad \varphi_2=-q_2+r_2,\quad \boldsymbol{\eta}_1=-\boldsymbol{p},\quad \boldsymbol{\eta}_2=\boldsymbol{s}_1,\quad \varphi_3=u_t,\quad \varphi_4=v_t.$$

Then we have

$$\int_K u_t(-q_1+r_1)dK=-\int_K \boldsymbol{s}_1\cdot\nabla(-q_1+r_1)dK+\int_{\partial K}\widehat{\boldsymbol{s}_1\cdot\nu}(-q_1+r_1)ds, \tag{3.8}$$

$$\int_K v_t(-q_2+r_2)dK=\int_K -b(u,v)(-q_2+r_2)(-q_2+r_2)/\rho dK, \tag{3.9}$$

$$-\int_K \boldsymbol{s}_1\cdot\boldsymbol{p}dK=-\int_K b(u,v)\boldsymbol{p}\cdot\boldsymbol{p}dK, \tag{3.10}$$

$$\int_K \boldsymbol{p}\cdot\boldsymbol{s}_1 dK=-\int_K(-q_1+r_1)(\nabla\cdot\boldsymbol{s}_1)dK+\int_{\partial K}(-\widehat{q_1}+\widehat{r_1})(\boldsymbol{s}_1\cdot\nu)ds, \tag{3.11}$$

$$\int_K q_1u_t dK=-\gamma\int_K \boldsymbol{w}_1\cdot\nabla u_t dK+\int_{\partial K}\gamma\widehat{\boldsymbol{w}_1\cdot\nu}u_t ds, \tag{3.12}$$

$$\int_K q_2v_t dK=-\gamma\int_K \boldsymbol{w}_2\cdot\nabla v_t dK+\int_{\partial K}\gamma\widehat{\boldsymbol{w}_2\cdot\nu}v_t ds. \tag{3.13}$$

Summing up the equations (3.5)-(3.13), we obtain

$$\begin{aligned}&\int_K\{\gamma(\boldsymbol{w}_{1t}\cdot\boldsymbol{w}_1+\boldsymbol{w}_{2t}\cdot\boldsymbol{w}_2)+\Psi_u u_t+\Psi_v v_t\}dK\\&+\int_K b(u,v)(-q_2+r_2)(-q_2+r_2)/\rho dK+\int_K b(u,v)\boldsymbol{p}\cdot\boldsymbol{p}dK\\=&-\int_{\partial K}\boldsymbol{s}_1\cdot\nu(-q_1+r_1)ds+\int_{\partial K}\widehat{\boldsymbol{s}_1\cdot\nu}(-q_1+r_1)ds+\int_{\partial K}(-\widehat{q_1}+\widehat{r_1})(\boldsymbol{s}_1\cdot\nu)ds\end{aligned}$$

Table 1: Accuracy test for the AC/CH system with the exact solution (4.1). Uniform meshes with J cells at time $t=0.5$.

		u				v			
	J	L^2 error	order	L^∞ error	order	L^2 error	order	L^∞ error	order
P^0	10	4.07E-01	–	1.04E-00	–	8.24E-02	–	1.87E-01	–
	20	1.67E-01	1.29	5.24E-01	1.00	4.09E-02	1.01	9.54E-02	0.97
	40	7.81E-02	1.10	2.54E-01	1.04	2.04E-02	1.00	4.77E-02	1.00
	80	3.84E-02	1.03	1.26E-01	1.00	1.02E-02	1.00	2.38E-02	1.00
P^1	10	8.42E-02	–	3.68E-01	–	1.35E-02	–	4.93E-02	–
	20	1.99E-02	2.08	8.99E-02	2.03	3.37E-03	2.01	1.24E-02	1.99
	40	4.91E-03	2.02	2.23E-02	2.01	8.41E-04	2.00	3.12E-03	2.00
	80	1.22E-03	2.00	5.57E-03	2.00	2.10E-04	2.00	7.79E-04	2.00
P^2	10	6.68E-03	–	3.42E-02	–	5.96E-04	–	2.55E-03	–
	20	7.92E-04	3.08	3.96E-03	3.11	7.35E-05	3.02	3.11E-04	3.03
	40	9.76E-05	3.02	5.06E-04	2.97	9.16E-06	3.01	3.91E-05	2.99
	80	1.22E-05	3.01	6.35E-05	2.99	1.14E-06	3.00	4.89E-06	3.00
P^3	10	8.49E-04	–	3.38E-03	–	4.35E-05	–	1.57E-04	–
	20	5.60E-05	3.92	2.23E-04	3.92	2.76E-06	3.98	1.01E-05	3.96
	40	3.55E-06	3.98	1.41E-05	3.98	1.73E-07	3.99	6.33E-07	3.99
	80	2.22E-07	4.00	8.90E-07	3.99	9.51E-09	4.19	3.73E-08	4.08

$$-\gamma\int_{\partial K}u_t(\boldsymbol{w}_1\cdot\nu)ds+\gamma\int_{\partial K}\widehat{u_t}(\boldsymbol{w}_1\cdot\nu)ds+\int_{\partial K}\gamma\widehat{\boldsymbol{w}_1\cdot\nu}u_t ds$$
$$-\gamma\int_{\partial K}v_t(\boldsymbol{w}_2\cdot\nu)ds+\gamma\int_{\partial K}\widehat{v_t}(\boldsymbol{w}_2\cdot\nu)ds+\int_{\partial K}\gamma\widehat{\boldsymbol{w}_2\cdot\nu}v_t ds.$$

Summing up the cell entropy equalities, with the numerical fluxes (3.3) and the boundary conditions (3.4), we get

$$\int_\Omega\{\gamma(\boldsymbol{w}_{1t}\cdot\boldsymbol{w}_1+\boldsymbol{w}_{2t}\cdot\boldsymbol{w}_2)+\Psi_u u_t+\Psi_v v_t\}dK$$
$$+\int_\Omega b(u,v)(-q_2+r_2)(-q_2+r_2)/\rho dK+\int_\Omega b(u,v)\boldsymbol{p}\cdot\boldsymbol{p}dK=0.$$

For $b(u,v)\geq 0$, we obtain

$$\frac{d}{dt}\int_K\left\{\frac{\gamma}{2}(\boldsymbol{w}_1\cdot\boldsymbol{w}_1+\boldsymbol{w}_2\cdot\boldsymbol{w}_2)+\Psi\right\}dK\leq 0. \tag{3.14}$$

This completes the proof of this proposition. □

Remark 3.1. Although the proof of the energy stability in Proposition 3.1 follows the similar line as in [10], the result of Proposition 3.1 is for the general AC/CH system. The result in [10] is only for the CH equation which is a special case of the AC/CH system.

Table 2: Accuracy test for the AC/CH system with the exact solution (4.2). Uniform meshes with J cells at time $t=0.5$.

		u				v			
	J	L^2 error	order	L^∞ error	order	L^2 error	order	L^∞ error	order
P^0	10	4.02E-02	–	8.19E-02	–	1.49E-03	–	3.43E-03	–
	20	1.59E-02	1.33	3.52E-02	1.22	7.47E-04	1.00	1.74E-03	0.98
	40	7.32E-03	1.12	1.68E-02	1.06	3.74E-04	1.00	8.72E-04	1.00
	80	3.57E-03	1.03	8.31E-02	1.01	1.87E-04	1.00	4.36E-04	1.00
P^1	10	7.92E-03	–	2.83E-02	–	2.02E-04	–	7.09E-04	–
	20	1.93E-03	2.04	6.92E-03	2.03	5.05E-05	2.00	1.81E-04	1.97
	40	4.79E-04	2.01	1.73E-03	2.00	1.26E-05	2.00	4.56E-05	1.99
	80	1.19E-04	2.00	4.33E-04	1.99	3.15E-06	2.00	1.14E-05	2.00
P^2	10	8.16E-04	–	3.45E-03	–	1.07E-05	–	4.58E-05	–
	20	1.02E-04	3.00	4.22E-04	3.03	1.34E-06	3.00	5.69E-06	3.01
	40	1.27E-05	3.00	5.40E-05	2.96	1.67E-07	3.00	7.16E-07	2.99
	80	1.59E-06	3.00	6.79E-06	2.99	2.09E-08	3.00	8.97E-08	3.00
P^3	10	6.58E-05	–	3.00E-04	–	4.38E-07	–	1.99E-06	–
	20	4.15E-06	3.99	1.95E-05	3.95	2.74E-08	4.00	1.28E-07	3.95
	40	2.60E-07	4.00	1.21E-06	4.01	1.72E-09	4.00	8.08E-09	3.99
	80	1.62E-08	4.00	7.60E-08	3.99	1.08E-10	3.99	4.64E-10	4.13

4 Numerical results

In this section we perform numerical experiments of the LDG method applied to the AC/CH system. Time discretization is by the forward Euler method with a suitably small Δt for stability. Since $\Delta t=\mathcal{O}(h^4)$ for the stability constraint, accuracy is maintained up to fourth order. We will not address the issue of time discretization efficiency in this paper. All the computations were performed in double precision. We have verified with the aid of successive mesh refinements, that in all cases, the results shown in the figures are numerically convergent.

Example 4.1. In this example, we consider the accuracy test for the AC/CH system. Consider $\Omega=(0,4\pi)$, $\gamma=6$, $\alpha=11/2$, $\beta=1/2$ and $\rho=1.0$ with constant mobility $b=1$. We consider two cases with different value of θ.

`Case 1.` $\theta=0$. In this case, the AC/CH system decouples to the AC equation and the CH equation. We take the exact solution of

$$u(x,t)=e^t\cos(0.5x)-e^{-0.5t}\sin(x),\quad v(x,t)=e^{-t}\cos(0.5x). \tag{4.1}$$

The L^2 and L^∞ errors and the numerical orders of accuracy at time $t=0.5$ with uniform meshes are contained in Table 1.

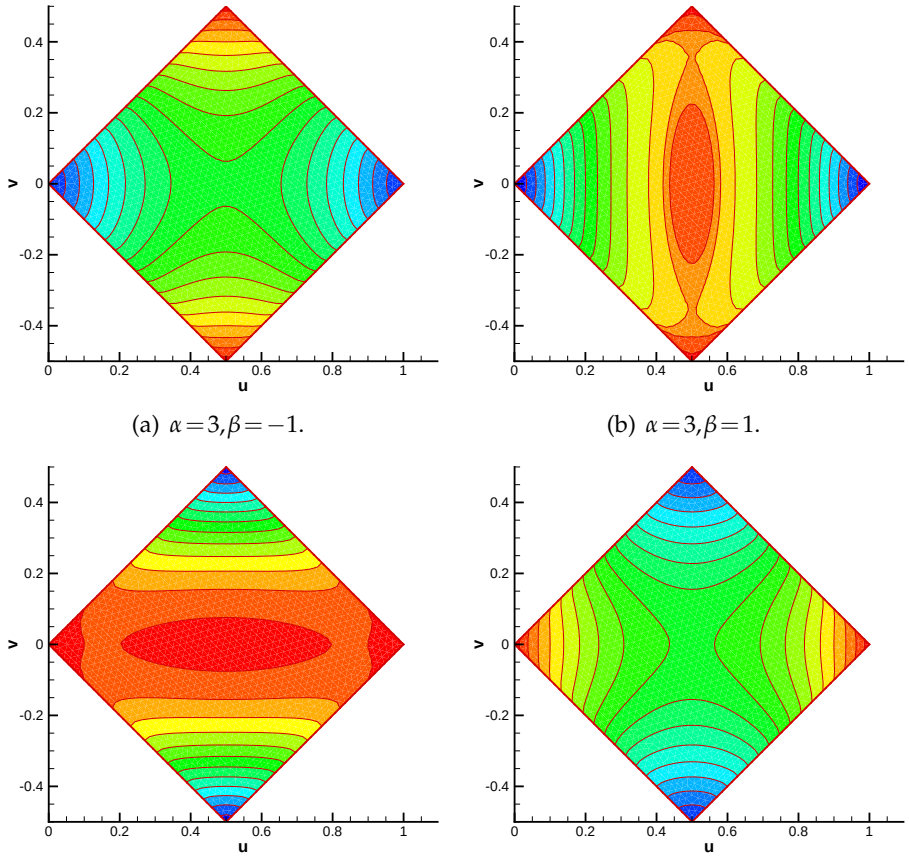

(a) $\alpha=3,\beta=-1$. (b) $\alpha=3,\beta=1$.

(c) $\alpha=1,\beta=3$. (d) $\alpha=-1,\beta=3$.

Figure 1: The homogeneous free energy Ψ with different α,β in Example 4.2.

`Case 2.` $\theta=0.1$. We take the exact solution of

$$u(x,t)=0.5-e^{-2-\frac{t}{2}}\sin(x),\quad v(x,t)=e^{-4-t}\cos(0.5x) \tag{4.2}$$

for the AC/CH system with the source term f, where f is a given function so that (4.2) is the exact solution. In this case, the AC/CH system is still coupled. The L^2 and L^∞ errors and the numerical orders of accuracy at time $t=0.5$ with uniform meshes are contained in Table 2.

We can see that the method with P^k elements gives (k+1)-th order of accuracy in both L^2 and L^∞ norms.

Example 4.2. Consider $\Omega=(0,1)$, $\theta=0.1$, $\epsilon=0.1$ and $\rho=0.08$ with degenerate mobility (2.2) and constant mobility $b=1/16$ respectively. The initial condition

$$(u^0,v^0)=(0.55+\delta_u,\delta_v),$$

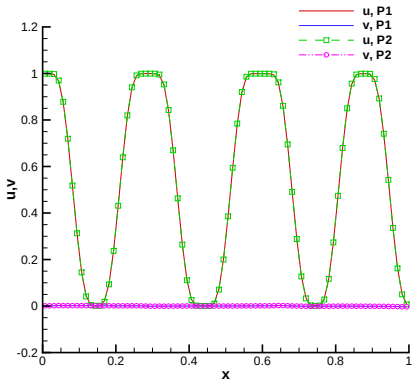

(a) $\alpha=3,\beta=-1$ with degenerate mobility (2.2), $t=2$.

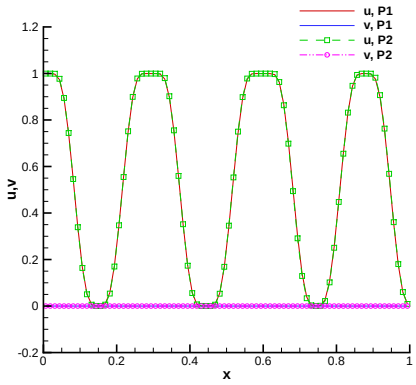

(b) $\alpha=3,\beta=-1$ with constant mobility $b=\frac{1}{16}$, $t=2$.

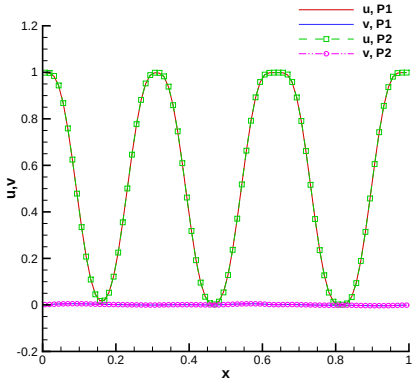

(c) $\alpha=3,\beta=1$ with degenerate mobility (2.2) $t=2$.

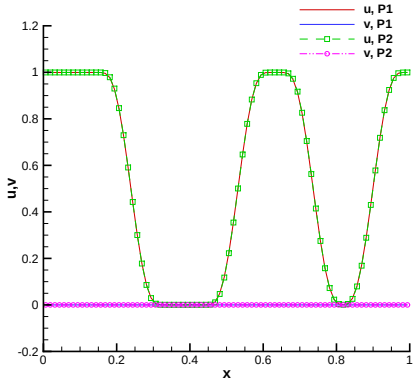

(d) $\alpha=3,\beta=1$ with constant mobility $b=\frac{1}{16}$, $t=6$.

Figure 2: The numerical solutions of the AC/CH system in Example 4.2. P^1 and P^2 element on uniform mesh with 80 cells.

where δ_u,δ_v are random with

$$\max(\|\delta_u\|_\infty,\|\delta_v\|_\infty)\leq 0.05. \tag{4.3}$$

We simulate the AC/CH system with the following different parameters: 1. $\alpha=3$, $\beta=-1$ and $\gamma=\frac{1}{6}\epsilon^2$; 2. $\alpha=3$, $\beta=1$ and $\gamma=\frac{1}{3}\epsilon^2$; 3. $\alpha=1$, $\beta=3$ and $\gamma=\frac{1}{3}\epsilon^2$; 4. $\alpha=-1$, $\beta=3$ and $\gamma=\frac{1}{6}\epsilon^2$.

In Fig. 1, we plot the corresponding homogeneous free energy Ψ in (2.4). We see the energy Ψ has two global minimizers located at (0,0) and (0,1) when $(\alpha,\beta)=(3,\pm1)$, and two global minimizers located at $(0.5,\pm0.5)$ when $(\alpha,\beta)=(\pm1,3)$. We use P^1 and P^2 elements and show the results with the P^2 element and a uniform mesh with 80 cells in Fig. 1. The simulations are stopped when the obtained profiles do not change for a long time (the maximum residue is less than 10^{-6}).

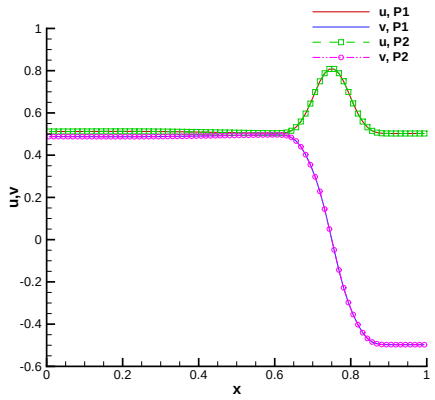

(a) $\alpha=1,\beta=3$ with degenerate mobility (2.2), $t=8$.

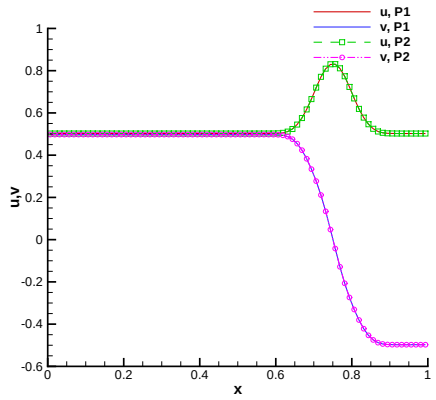

(b) $\alpha=1,\beta=3$ with constant mobility $b=\frac{1}{16}$, $t=4$.

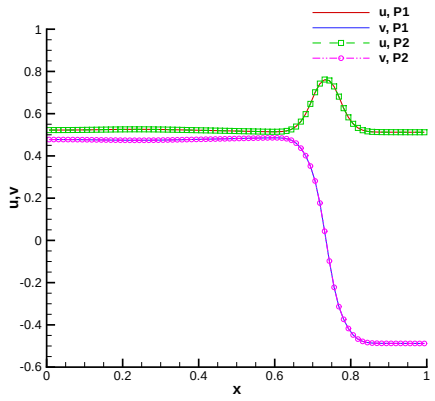

(c) $\alpha=-1,\beta=3$ with degenerate mobility (2.2) $t=8$.

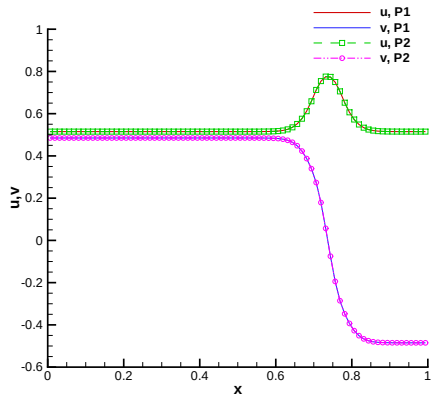

(d) $\alpha=-1,\beta=3$ with constant mobility $b=\frac{1}{16}$, $t=6$.

Figure 3: The numerical solutions of the AC/CH system in Example 4.2. P^1 and P^2 element on uniform mesh with 80 cells.

In Figs. 2 and 3, we show the numerical results in different cases, which satisfy the constraints (1.2). We have the following observations:

- As shown in Fig. 2, the numerical solution converges to the global minimizers $(0,0)$ and $(0,1)$ of the free energy Ψ when $(\alpha,\beta)=(3,\pm1)$.
- Similarly, the numerical solution converges to the global minimizers $(0.5,\pm0.5)$ of Ψ in Fig. 3. The degenerate mobility $b(u,v)$ in (2.2) has four roots $(0.5,\pm0.5)$, $(0,0)$ and $(0,1)$, which are global minimizers of Ψ.
- As shown in Figs. 2 and 3, the diffusion in the degenerate mobility cases is vanishing in pure phases ($(0,0)$ and $(0,1)$) and in a perfectly ordered environment ($(0.5,\pm0.5)$). The solution is changing more slowly compared with the constant mobility cases.

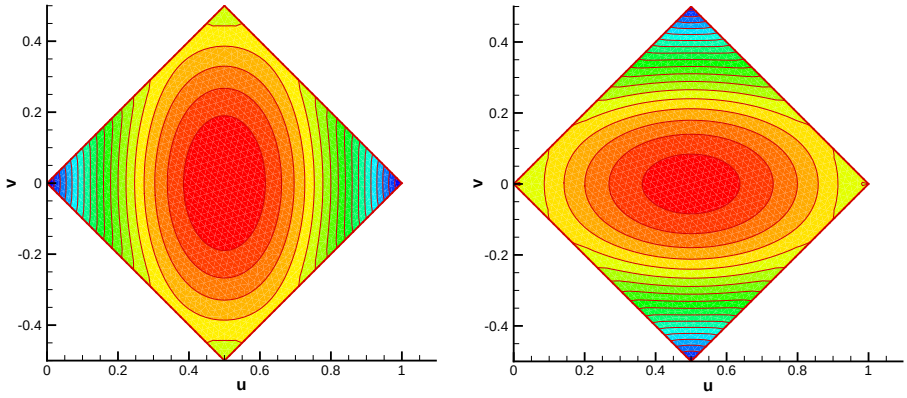

(a) $\alpha=4,\beta=2$. (b) $\alpha=2,\beta=4$.

Figure 4: The homogeneous free energy Ψ with different α, β in Example 4.3.

Example 4.3. To show the capability of the method, we consider the following $2D$ examples in $\Omega=(0,1)\times(0,1)$, $\gamma=5\times10^{-3}$, $\theta=0.1$ with degenerate and constant mobility respectively. The initial condition $(u^0,v^0)=(0.55+\delta_u,\delta_v)$, where δ_u,δ_v are random which satisfies (4.3). We consider the following cases with the global minimizers of the free energy Ψ located at pure phases or ordered environment:

1. $\alpha=4$, $\beta=2$, $\rho=0.001$ with degenerate mobility (2.2);
2. $\alpha=4$, $\beta=2$, $\rho=0.001$ with constant mobility $b=1/16$, which is the maximum of the degenerate mobility;
3. $\alpha=2$, $\beta=4$, $\rho=0.08$ with degenerate mobility (2.2);
4. $\alpha=2$, $\beta=4$, $\rho=0.08$ with constant mobility $b=1/16$.

The corresponding free energy Ψ is plotted in Fig. 4. When α=4, β=2, the global minimizers Ψ are located at $(0,0)$ and $(0,1)$. The global minimizers of Ψ are located at $(0.5,\pm0.5)$ if $\alpha=2$, $\beta=4$. We use P^1 element and a uniform mesh with 40×40 cells.

The numerical results are given in Figs. 5, 6, 7 and 8 for the four different cases. In each case, the numerical results satisfy the constraints (1.2) and converge to the corresponding global minimizer of the free energy Ψ.

- In Figs. 5 and 6 where $\alpha>\beta$, initially both spinodal decomposition and order-disorder type instabilities occur. However, as the final equilibrium is approached, only separation into two terminal phases is seen.
- In Figs. 7 and 8 where $\alpha<\beta$, ordering without initial phase separation occurs and the final equilibrium corresponds to a mixture of ordered and terminal phases. There is a delayed spinodal decomposition that begins only after some ordering has occurred.
- As in the 1D example, we find the solution with the degenerate mobility (2.2) changes more slowly than the solution with the constant mobility, which is the maximum of the degenerate mobility.

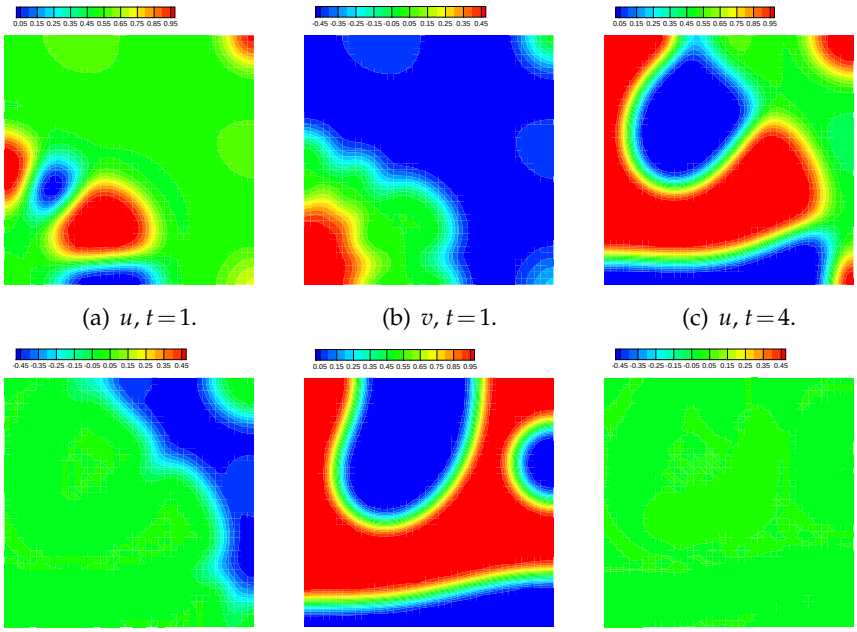

(a) u, $t=1$. (b) v, $t=1$. (c) u, $t=4$.

(d) v, $t=4$. (e) u, $t=6$. (f) v, $t=6$.

Figure 5: The numerical solutions of the AC/CH system in Example 4.3 with $\alpha=4$, $\beta=2$ and the degenerate mobility (2.2). P^1 element on uniform mesh with 40×40 cells.

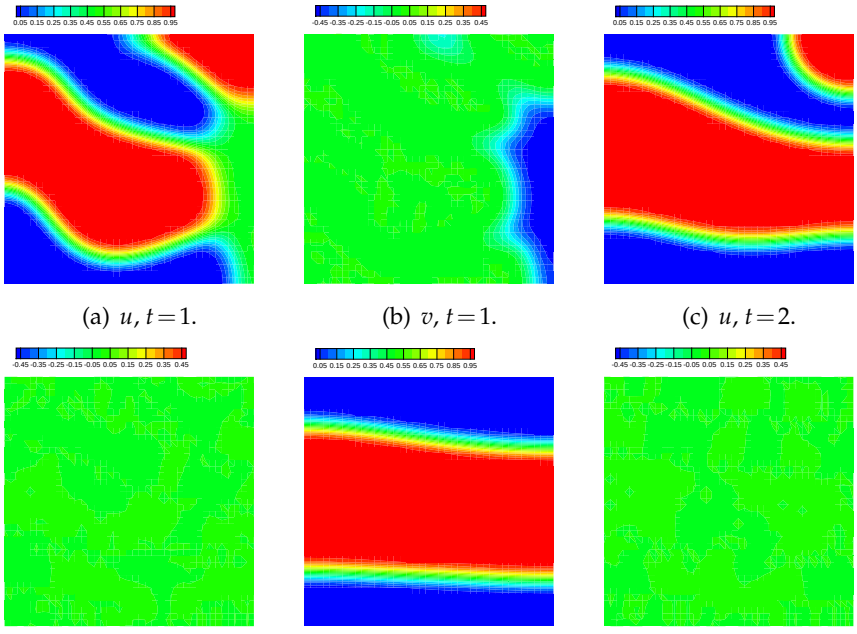

(a) u, $t=1$. (b) v, $t=1$. (c) u, $t=2$.

(d) v, $t=2$. (e) u, $t=4$. (f) v, $t=4$.

Figure 6: The numerical solutions of the AC/CH system in Example 4.3 with $\alpha=4$, $\beta=2$ and the constant mobility $b=\frac{1}{16}$. P^1 element on uniform mesh with 40×40 cells.

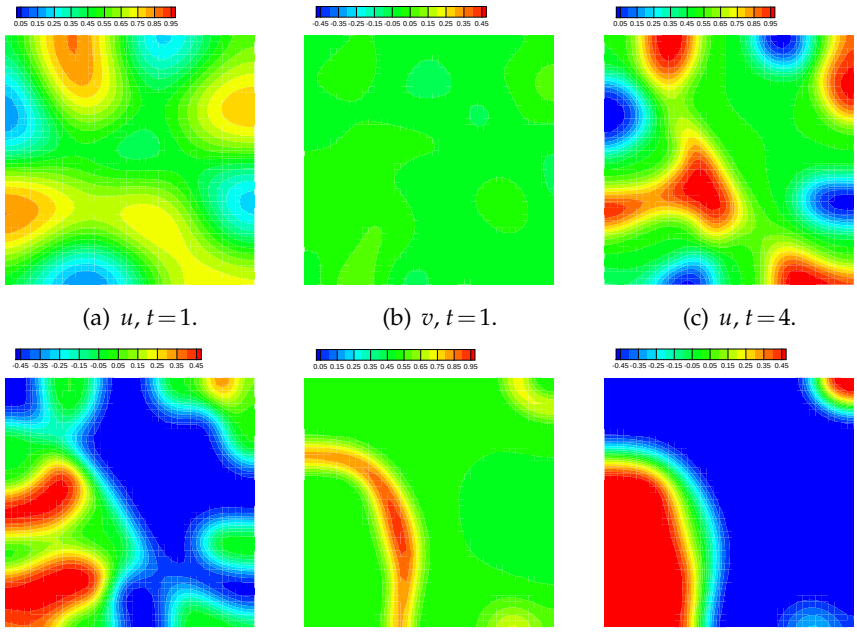

(a) $u, t=1$. (b) $v, t=1$. (c) $u, t=4$.

(d) $v, t=4$. (e) $u, t=8$. (f) $v, t=8$.

Figure 7: The numerical solutions of the AC/CH system in Example 4.3 with $\alpha=2$, $\beta=4$ and the degenerate mobility (2.2). P^1 element on uniform mesh with 40×40 cells.

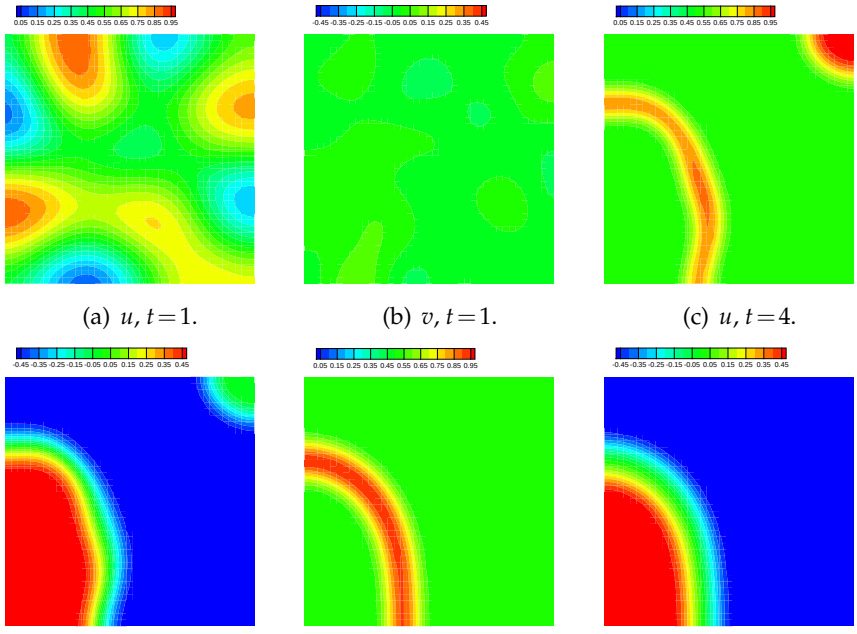

(a) $u, t=1$. (b) $v, t=1$. (c) $u, t=4$.

(d) $v, t=4$. (e) $u, t=8$. (f) $v, t=8$.

Figure 8: The numerical solutions of the AC/CH system in Example 4.3 with $\alpha=2$, $\beta=4$ and the constant mobility $b=\frac{1}{16}$. P^1 element on uniform mesh with 40×40 cells.

5 Conclusion

We have discussed the application of local discontinuous Galerkin methods to solve the Allen-Cahn/Cahn-Hilliard system. The energy stability is proven for the general nonlinear case. Numerical examples for one-dimensional and two dimensional cases are given to illustrate the accuracy and capability of the methods. These results indicate that the LDG method is a good tool for solving such nonlinear equations in mathematical physics.

Acknowledgments

The research of the first author is supported in part by NSFC grant 10601055. The research of the second author is supported by NSFC grant 10601055. The research of the third author is supported in part by NSFC grant 10671190 during his visit to the Department of Mathematics, University of Science and Technology of China, Hefei, Anhui 230026, P.R. China. Additional support is provided by NSF grant DMS-0510345.

References

[1] J.W. Barrett and J.F. Blowey, *Finite element approximation of a degenerate Allen-Cahn/Cahn-Hilliard system*, SIAM J. Numer. Anal., **39** (2001), pp.1598-1624.
[2] J.W. Barrett and J.F. Blowey, *Finite element approximation of an Allen-Cahn/Cahn-Hilliard system*, IMA J. Numer. Anal., **22** (2002), pp.11-71.
[3] J.W. Cahn and A. Novick-Cohen, Evolution equations for phase separation and ordering in binary alloys, J. Stat. Phys., **76** (1994), pp. 877-909.
[4] B. Cockburn, *Discontinuous Galerkin methods for methods for convection-dominated problems*, in *High-Order Methods for Computational Physics*, T.J. Barth and H. Deconinck, editors, Lecture Notes in Computational Science and Engineering, volume 9, Springer, 1999, pp.69-224.
[5] B. Cockburn and C.-W. Shu, *The local discontinuous Galerkin method for time-dependent convection-diffusion systems*, SIAM J. Numer. Anal., **35** (1998), pp.2440-2463.
[6] B. Cockburn and C.-W. Shu, *Runge-Kutta Discontinuous Galerkin methods for convection-dominated problems*, J. Sci. Comput., **16** (2001), pp.173-261.
[7] B. Cockburn and C.-W. Shu, *Foreword for the special issue on discontinuous Galerkin method*, J. Sci. Comput., **22-23** (2005), pp.1-3.
[8] C. Dawson, *Foreword for the special issue on discontinuous Galerkin method*, Comput. Meth. Appl. Mech. Engin., **195** (2006), p.3183.
[9] D. Levy, C.-W. Shu and J. Yan, *Local discontinuous Galerkin methods for nonlinear dispersive equations*, J. Comput. Phys., **196** (2004), pp.751-772.
[10] Y. Xia, Y. Xu and C.-W. Shu, *Local discontinuous Galerkin methods for the Cahn-Hilliard type equations*, J. Comput. Phys., **227** (2007), pp.472-491.
[11] Y. Xu and C.-W. Shu, *Local discontinuous Galerkin methods for nonlinear Schrödinger equations*, J. Comput. Phys., **205** (2005), pp.72-97.
[12] Y. Xu and C.-W. Shu, *Local discontinuous Galerkin methods for two classes of two dimensional nonlinear wave equations*, Physica D, **208** (2005), pp.21-58.
[13] J. Yan and C.-W. Shu, *A local discontinuous Galerkin method for KdV type equations*, SIAM J. Numer. Anal., **40** (2002), pp.769-791.